Testing and simulation of a solar diffusion-absorption refrigeration system for low-cost solar cooling in India

James Freeman[1], Ahmad Najjaran[1], Robert Edwards[2], Michael Reid[2], Richard Hall[3], Alba Ramos[1], Christos N. Markides[1]

[1] Clean Energy Processes (CEP) Laboratory, Imperial College London, London (UK)

[2] Solar-Polar Ltd., Peterborough (UK)

[3] Energy Transitions Ltd., Pontypridd (UK)

Abstract

Solar cooling technologies have the potential to improve crop and vaccine supply chain management in areas with unreliable access to an electricity distribution network. The diffusion absorption refrigeration (DAR) cycle is a technology of interest for cooling in rural areas and developing countries due to its low capital cost, low maintenance requirements, and unique design in which the requirement for electrically-driven components are fully omitted. The main feature of DAR systems is a thermally driven bubble pump that is used to circulate the refrigerant and absorbent fluid components around the system. In this paper, we present results from a laboratory DAR system operating over a range of pressures and heat input rates with ammonia-water-hydrogen as the working fluid. By reducing the system pressure from 21 bar to 14 bar, a 17% increase in maximum coefficient of performance (COP) is reported, and the system start-up time is reduced by up to 58%. The results are used to calibrate a thermal model of a solar-DAR system, which is then used to determine the optimal system pressure and solar collector array configuration for summer operation in the location of Chennai, India.

Keywords: Solar cooling, diffusion absorption refrigeration, cold chain, solar thermal collectors

1. Introduction

The DAR cycle was patented by von Platen and Munters in 1928. Its principle of operation differs from that of absorption refrigeration systems based on dual-pressure cycles and binary fluid mixtures in that it is designed for "single-pressure" operation enabled by a third component, which imposes different partial pressures on the refrigerant. The basic design has changed little since the early systems, which use ammonia-water-hydrogen as the working fluid at system pressures of 20-25 bar to utilize thermal energy typically at temperatures of 180-250 ˚C.

A DAR system schematic is shown in Fig. 1. An ammonia-water solution is heated in the generator (1-2), and boils so that the depleted liquid solution (3) is lifted by the ammonia-rich vapour (4) to the top of the bubble pump. The vapour rises to the rectifier, where most of the remaining water is separated out (5), leaving a near-pure ammonia vapour (6). The ammonia returns to the liquid phase in the condenser (6-7a) and is precooled (7a-9) before entering the evaporator, where it evaporates and diffuses into a reduced partial pressure hydrogen environment, extracting heat from the evaporator's surroundings (9-10). Any uncondensed vapour leaving the condenser bypasses the evaporator entirely (7b-10). Saturated-vapour ammonia mixed with hydrogen exits the bottom of the evaporator and enters the reservoir, then rises through the absorber column where it is absorbed by the downwards flowing weak solution introduced at the top (8a). The hydrogen meanwhile is not absorbed and rises back to the evaporator (8b) via a gas heat exchanger where it is pre-cooled by the downward flowing refrigerant. The liquid solution, having absorbed the ammonia from the upward-flowing gas, settles in the bottom of the reservoir before proceeding to the generator via the liquid heat exchanger (11-1).

Recent research has considered how the DAR cycle can be adapted for use in a lower temperature range with solar thermal collectors. Approaches considered include the use of alternative working fluids (Zohar *et al.* 2009, Ben Ezzine *et* al. 2010, Acuña *et al*., 2013) and the configuration of the generator and bubble pump (Zohar *et al*. 2008, Damak *et al*., 2010). The UK company Solar-Polar has recently developed a solar-DAR system for use in rural cold chain applications. A field-test of the system is currently in preparation at Anna University in Chennai, India (see Fig. 2), where fifteen modular roof-top units will be used to provide cooling to a 34 m^3 insulated cold store. Each unit provides a nominal 60-70 W of cooling from a 0.72 m^2 array of solar heat pipe collectors. A one-year monitoring study will be undertaken in order to assess the seasonal performance of the system.

doi:10.18086/swc.2017.28.07 Available at http://proceedings.ises.org

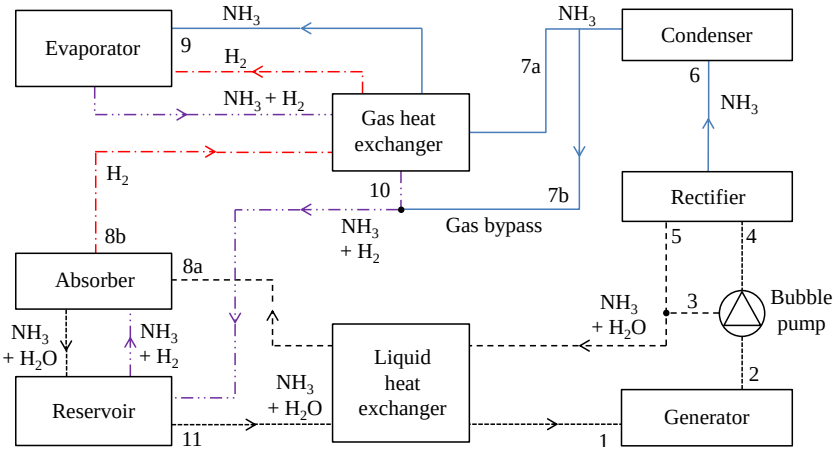

Fig. 1: Schematic diagram of the diffusion absorption refrigeration cycle showing the flows of the ammonia, water and hydrogen working fluid mixture components. For descriptions of the numbered cycle state points, refer to Fig. 3.

To ensure that the units in the pilot study are configured to provide maximum cooling output in Chennai conditions, a predictive model that can capture the performance of the system over diurnal and seasonal time-scales is an invaluable tool. The processes of the DAR cycle are well understood, however many of the models presented in the literature (Zohar *et al*. 2005, Starace and De Pascalis 2012, Taieb *et al*. 2016) use restrictive assumptions about the state of the system that are based on a limited range of operating conditions. In particular, there is a lack of experimentally-validated models for the ammonia-water-hydrogen DAR cycle operating over a wide range of system pressures and solution concentrations. The system pressure is an essential parameter for optimization in solar thermal applications, which represents a trade-off between the operating temperature and efficiency of the solar collector array, and the ability to reject heat from the cycle to the ambient air.

Fig. 2: Solar-Polar DAR demonstration system with heat pipe solar collector array, installed at Anna University campus, Chennai.

In this paper, the Solar-Polar DAR system will be used as the basis for a laboratory study in which the performance of the system will be characterized over a range of operating conditions. The experimental data will be used to calibrate a thermodynamic model of the system developed in earlier work (Freeman *et al*. 2016), and a whole-system solar-DAR model will then be used to simulate performance in the Chennai climate over a range of operating pressures and with various solar collector configurations.

2. Experimental methods

Steady-state tests were performed on the laboratory DAR units over a range of generator heat input powers ($\dot{Q}_{\mathrm{gen}}$) and system charge pressures (p_{ch}). In this paper, results will mostly be presented for a cooling delivery temperature (T_{cool}) of 5 ˚C. The main performance parameter of interest is the cooling power delivered by the DAR evaporator ($\dot{Q}_{\mathrm{evap}}$) and the coefficient of performance (COP), which is defined as the ratio of the cooling output delivered at the evaporator to the heat input provided to the generator. Therefore accurate measurements of both the heat input and cooling output from the system are required.

Heat was provided by five 9.5-mm diameter cartridge heaters, of similar dimensions to the condenser end of the heat pipe collectors used in the solar-DAR setup. The cartridge heaters were fitted into sockets welded to the outer surface of the generator tube. The full length of the bubble pump was insulated with 50 mm of rockwool insulation, while a larger thickness of 100 mm was used to insulate the generator and cartridge heaters. During each steady-state test, the electrical power to the cartridge heaters was maintained at a fixed value, set using an AC autotransformer (variac). The heater power was varied between 0-500 W at intervals of 50 W for each pressure level. Three system charge pressure settings were chosen for the experiments: (i) 14 bar; (ii) 17 bar; and (iii) 21 bar (absolute pressure, measured while the system was at rest under ambient temperature conditions).

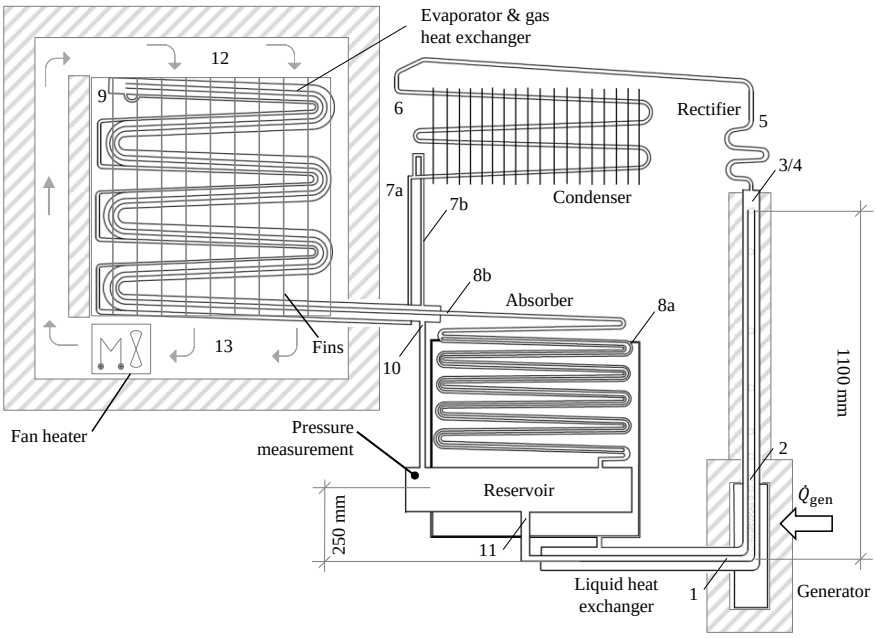

State points

1. Generator inlet	5. Rectifier	8a. Absorber, liquid inlet	11. Reservoir outlet
2. Generator outlet	6. Condenser inlet	8b. Absorber, gas outlet	12. Evaporator air on
3. Bubble pump outlet (liquid)	7a. Condenser outlet (liquid)	9. Evaporator inlet	13. Evaporator air off
4. Bubble pump outlet (vapour)	7b. Condenser outlet (gas bypass)	10. Evaporator outlet	

Fig. 3: Layout of the laboratory DAR system showing major components and numbered state points representing the locations of temperature measurements on the system.

In order to measure the cooling power $\dot{Q}_{\mathrm{evap}}$, a box was constructed around the evaporator using 100 mm thick layers of rigid polyurethane insulation. The internal dimensions of the cold box were 710 × 360 × 110 mm, giving an internal volume of 0.0281 m^3. Sealant was applied around all pipe penetrations in order to minimize air leakage to or from the surroundings. A small electric fan heater placed inside the box was used to control the temperature of the air delivered across the surface of the evaporator. Air was delivered in a downward direction via an insulated channel running along the edge of the box and was distributed between parallel aluminium fins attached to the outer surface of the steel evaporator tubing. The power delivered by the fan heater was controlled so that the "air off" temperature measured at the bottom of the evaporator was maintained at a constant value of 5 °C. Heat losses from the box were estimated in the final COP calculations by assuming a U-value of 0.24 W m^{-2} K^{-1} and an air leakage rate of 0.2 air changes per hour from the cold box.

Detailed temperature measurements were taken on each system sub-component in order to evaluate assumptions used in the thermodynamic model of the cycle (see Section 3.1). For some of the locations, measurement of fluid temperatures was challenging, for example in the concentric tube (pipe-in-pipe) heat exchangers in the evaporator and bubble pump. The apparatus was modified to include thermowells welded into the pipework so that fluid temperatures in the inner tube of the bubble pump could be measured more accurately at locations 2 and 3. Elsewhere in the system, most fluid temperatures were estimated from measurements in contact with the outer surfaces of the steel tubes. A direct measurement of system pressure during the tests was also provided by a pressure transducer located at the fluid reservoir. For each run, the system was operated under steady-state

conditions for a period of one hour while temperatures, pressure and electrical input power to the cartridge heaters and fan heater were measured at intervals of 1 second. Air temperature in the laboratory was maintained at approximately 25 ºC, although some variation of ± 2 ºC was found to occur between the tests.

Previous experimental studies by Mazouz *et al.* (2014) and Ben Jemaa *et al.* (2016), among others, have noted that the starting characteristic of DAR systems varies significantly with heat input rate. During the start-up process, the solution in the generator is heated until it transitions from nucleate boiling to a state where significant bubble coalescence takes place to provide lifting of the liquid solution through the entire length of the bubble pump. Shelton and White (2002) and Hanafizadeh *et al.* (2014) have discussed the conditions under which the bubble pump processes are dominated by slug flow or churn flow regimes. It is important to consider the dynamic behaviour of the system in any situation where the heat source is intermittent (such as solar applications), and therefore in the present work the temperature profiles of the generator during start-up will be used to determine the thermal capacity and minimum starting temperature under various operational settings.

3. Modelling methodology

A model of the solar-DAR system was developed to evaluate its performance under realistic climatic conditions and to select the most appropriate operational settings for the chosen location. In this paper, the model is used to investigate the optimal system pressure and solar collector array configuration for summer operation in Chennai. The sub-models of the DAR cycle and the solar collector sub-systems are described in the following sections.

3.1. DAR system sub-model

The thermodynamic model of the DAR cycle is based on the equations of Starace and De Pascalis (2012), and consists of 6 lumped sub-component models: (i) generator and bubble pump; (ii) rectifier; (iii) condenser; (iv) evaporator; (v) absorber; and (vi) liquid-solution heat exchanger. The energy balances for each component are shown in Eqs. 1-6, where $\dot{m}$ is mass flow rate in kg s^{-1}, $\dot{Q}$ is heat flow rate in W, h is specific enthalpy in J kg^{-1}, and "ig" denotes hydrogen (inert gas). The numbered state points correspond to those shown in Figs. 1 and 3.

$$\dot{Q}_{\mathrm{gen}} = \dot{m}_3 h_3 + \dot{m}_4 h_4 - \dot{m}_1 h_1 + \dot{Q}_{\mathrm{bp,loss}}, \quad \text{(eq. 1a)}$$

$$\dot{Q}_{\mathrm{bp,loss}} = \dot{m}_3 [h_3 - h_{\mathrm{l}}(T_2)] + \dot{m}_4 [h_4 - h_v(T_2)], \quad \text{(eq. 1b)}$$

$$\dot{Q}_{\mathrm{rect}} = \dot{m}_5 h_5 + \dot{m}_6 h_6 - \dot{m}_4 h_4, \quad \text{(eq. 2)}$$

$$\dot{Q}_{\mathrm{cond}} = \dot{m}_6 (h_7 - h_6), \quad \text{(eq. 3)}$$

$$\dot{Q}_{\mathrm{evap}} = \dot{m}_9 (h_{10} - h_{7\mathrm{a}}) + \dot{m}_{\mathrm{ig}} \left(h_{10,\mathrm{ig}} - h_{8\mathrm{b},\mathrm{ig}}\right), \quad \text{(eq. 4)}$$

$$\dot{Q}_{\mathrm{abs}} = \dot{m}_{11} h_{11} - \dot{m}_{10} h_{10} - \dot{m}_{8\mathrm{a}} h_{8\mathrm{a}} + \dot{m}_{\mathrm{ig}} h_{8\mathrm{b}} - \dot{m}_{\mathrm{ig}} h_{10,\mathrm{ig}} - \dot{m}_{7\mathrm{b}} h_{7\mathrm{b}}, \quad \text{(eq. 5)}$$

$$\dot{m}_3 h_3 + \dot{m}_5 h_5 - \dot{m}_{8\mathrm{a}} h_{8\mathrm{a}} = \dot{m}_1 (h_1 - h_{11}). \quad \text{(eq. 6)}$$

The thermodynamic properties of the ammonia-water mixtures were calculated using the correlations of Patek and Klomfar (1995), and REFPROP was used to calculate the properties of hydrogen. The DAR system models presented in Zohar *et al*. (2005) and Starace and De Pacalis (2012) require temperatures to be specified as inputs at several points in the cycle, including the inlet and/or outlet of the generator, condenser, evaporator and reservoir. The aim in the present work is to predict DAR performance using only the local climatic conditions, and information on the system charge pressure and thermal input provided from the solar collector array. Thus the experiments in this study will be used to characterize the performance of the various system components, and the following additional relations will be formulated for the bubble pump, rectifier and condenser:

$$T_2 = f(p, \dot{Q}_{\mathrm{gen}}), \quad \text{(eq. 7)}$$

$$T_6 = T_4 - \varepsilon_{\mathrm{rect}} (T_4 - T_{\mathrm{a}}), \quad \text{(eq. 8)}$$

$$\dot{Q}_{\mathrm{cond}} = UA_{\mathrm{cond}} \Delta T_{\mathrm{LMTD}}. \quad \text{(eq. 8)}$$

The following assumptions were also used: (i) the mass fraction of the rich ammonia-water solution entering the generator from the reservoir is fixed at 30% NH_3, with no hydrogen present; (ii) the preheated solution enters the generator as a saturated liquid; (iii) the refrigerant enters the condenser as a saturated vapour.

3.2. Solar collector sub-model

Two types of solar heat-pipe collector will be investigated for use with the DAR system. Collector 1, shown on the left in Fig. 2a, is a classic low-cost design consisting of a heat pipe with an aluminium fin inside an all-glass tube formed of two concentric layers. The annulus is evacuated, and a solar absorbing coating is applied to the inner glazed layer. Collector 2, shown on the right in Fig. 2a consists of a single-glazed tube with a fully evacuated core that contains a copper tube with a textured fin. The heat pipe is inserted inside the copper tube, and the solar absorbing coating is applied directly onto the surface of the metal fin. The former type of collector is easily mass-produced and available at very low costs in bulk quantities, while the latter tends to be more expensive due to the high-quality glass-to-metal seal required at the copper tube penetration point.

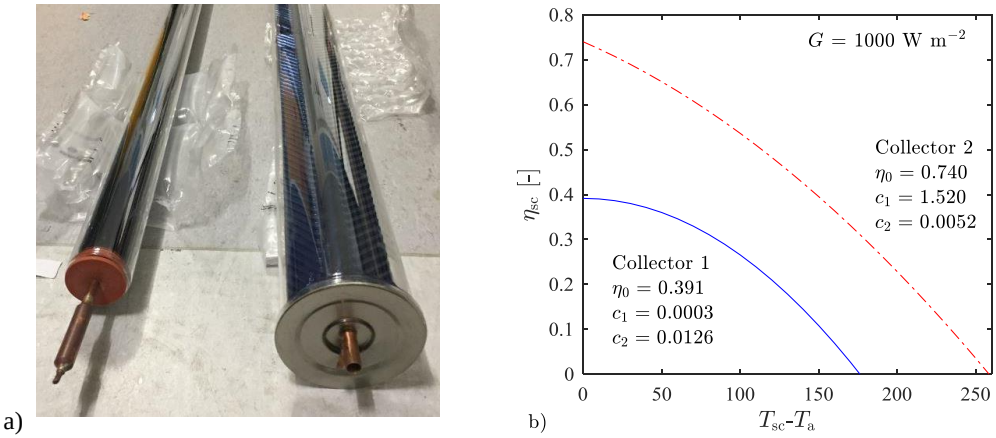

Fig. 4: (a) Photograph showing two heat pipe collector types investigated for use with the solar-DAR system: Collector 1 (left) and Collector 2 (right). (b) Efficiency curve plots for the two collectors (aperture area basis, G = 1000 W m^{-2}).

The efficiency curves for the two heat pipe collectors are compared in Fig. 2b, showing a higher zero-loss efficiency and stagnation temperature for Collector 2. The efficiency curve coefficients for Collector 2 were taken from a Solar Keymark performance test report (SPF, 2009). In the absence of existing performance data for Collector 1, the collector was tested in-house under irradiance conditions of 1000 W m^{-2} and a temperature range of 30-180 ˚C to obtain the efficiency curve coefficients η_0, c_1 and c_2 in Fig. 2b. The coefficients are used in the solar-DAR system model to calculate the collector's useful heat output $\dot{Q}_{\mathrm{sc}}$ as a function of the solar irradiance (direct and diffuse components G_{b} and G_{d}), collector temperature T_{sc} and ambient temperature T_{a}:

$$\dot{Q}_{sc} = \eta_0 A\left(K_{\theta,\mathrm{b}} G_{\mathrm{b}} + K_{\theta,\mathrm{d}} G_{\mathrm{d}}\right) - c_1 A(T_{\mathrm{sc}} - T_{\mathrm{a}}) - c_2 A(T_{\mathrm{sc}} - T_{\mathrm{a}})^2. \qquad \text{(eq. 9)}$$

The main dynamic component considered in the system model is associated with the thermal capacity C of DAR generator, which will be determined experimentally. The collector's effective thermal capacity is assumed to be small by comparison and is therefore not included in the model. The thermal conductance $(UA)_{\mathrm{gen}}$ between heat pipe collector and the DAR generator is also required to solve the following energy balance at 1-min intervals:

$$\dot{Q}_{\mathrm{sc}} = \dot{Q}_{\mathrm{gen}} + C\frac{dT_{\mathrm{gen}}}{dt} = (UA)_{\mathrm{sc-gen}}\left(T_{\mathrm{sc}} - T_{\mathrm{gen}}\right). \qquad \text{(eq. 10)}$$

3.3. Climate data for diurnal simulation

In the present study, the system operation will be simulated for a "peak solar" day in Chennai, India, using climate data published by ASHRAE (2001). The region of Chennai experiences high solar irradiance during the summer season, between the months of March to May. From June onwards, the weather is typically cloudier with periods of heavy rainfall. The day chosen for the simulation is the 3$^{\mathrm{rd}}$ of May.

4. Results and discussion

4.1. Experimental results – steady-state performance

Plots of cooling power and COP over the range of steady-state heat inputs are presented in Fig. 5 at the three system charge pressure settings 14 bar, 17 bar and 21 bar. It was found that for $p_{\mathrm{ch}} \geq 17$ bar, it was not possible to achieve the cooling delivery temperature of 5 ºC at $\dot{Q}_{\mathrm{gen}}$ values < 150 W.

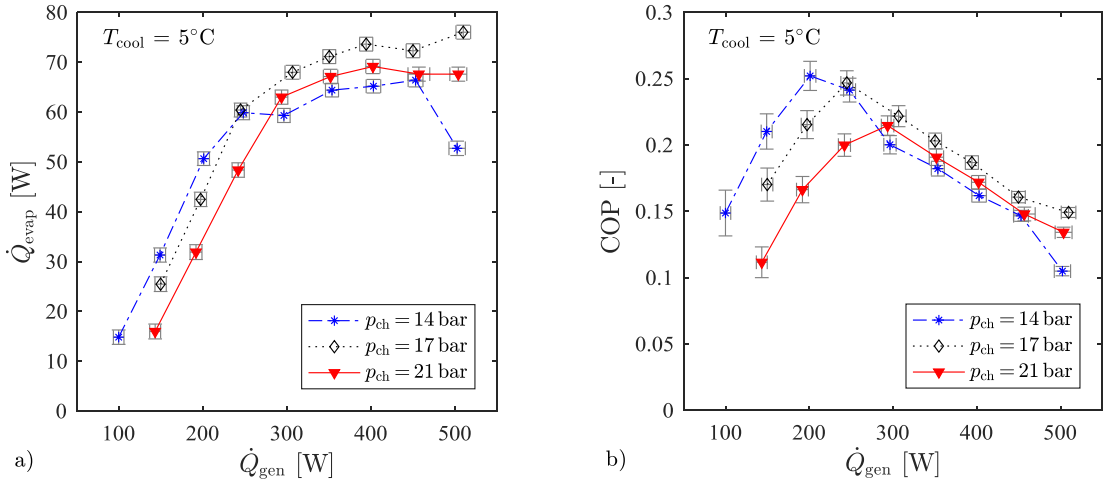

Fig. 5: Experimental results: (a) cooling power and (b) COP, at various charge pressures and for a cooling temperature of 5 °C.

The cooling output is shown to increase with generator heat input, however a change in the trend is observed at values of $\dot{Q}_{gen}$ around 200-300 W, that also corresponds to the peak COP of the system. The same behaviour was also observed in the study by Chen *et al.* (1996) who noted that for a further increase in heating input power beyond this point, liquid refrigerant begins to exit the evaporator.

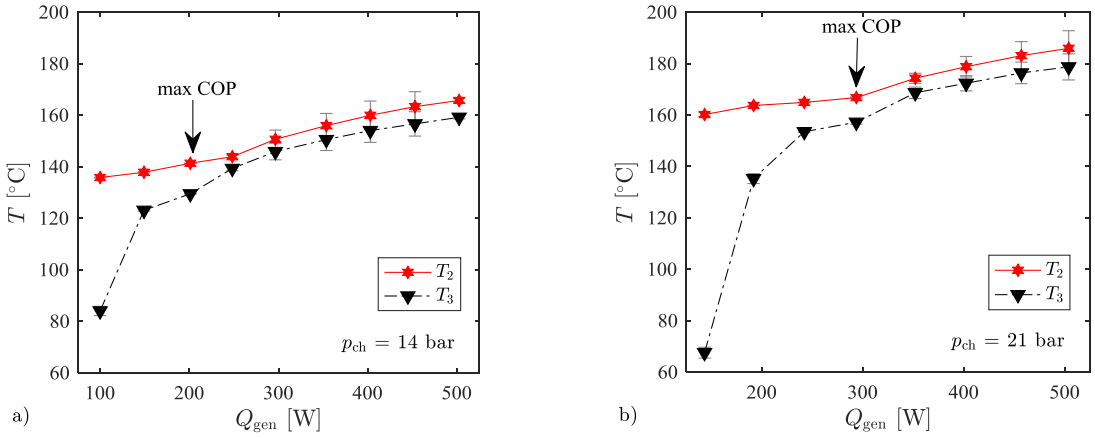

Fig. 6: Temperature at States 2 and 3 (generator outlet and top of the bubble pump, respectively), for system charge pressures of: (a) 14 bar and (b) 21 bar. Error bars denote standard deviation of measured values over the measurement period.

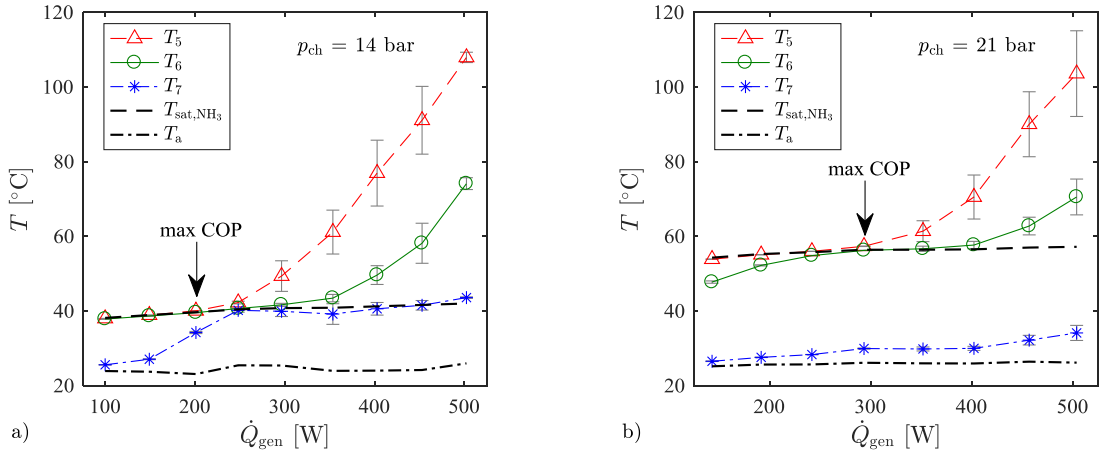

Fig. 7: Temperature at States 5, 6 and 7 (rectifier, condenser inlet and condenser outlet, respectively), for system charge pressures of: (a) 14 bar and (b) 21 bar. Also shown are the ambient air temperature T_a and the saturated liquid temperature of the refrigerant T_{sat,NH_3}. Error bars denote standard deviation of measured values over the measurement period.

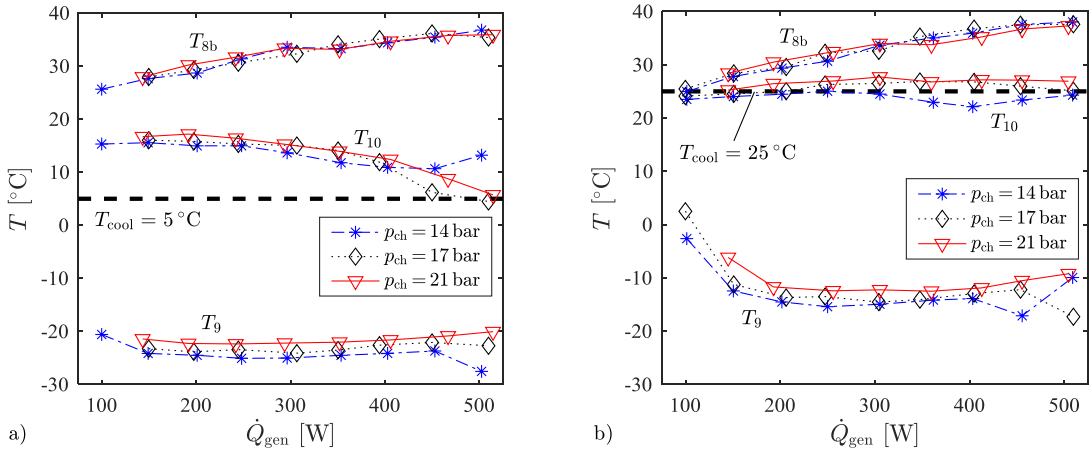

Fig. 8: Temperature at State 8b, 9 and 10 (absorber gas outlet, evaporator inlet and evaporator outlet, respectively), for cooling delivery temperatures (indicated by the dashed line) of: (a) 5 °C and (b) 25 °C, and for various values of p_{ch} and $\dot{Q}_{gen}$.

The mean temperatures measured along the bubble pump are plotted in Fig. 6. At low heat input rates, a large difference can be observed between the temperature at the top of the bubble pump T_3 and at the lower part of the bubble pump close to the generator T_2. At higher heat input rates this temperature difference is far smaller, indicating a change in flow regime that results in a lower level of heat dissipation according to Eq. 1b.

Full utilization of the rectifier and condenser is found to be a key factor in maximizing COP. Figure 7 shows the measured rectifier and condenser inlet and outlet temperatures; also indicated are the ambient air temperature and the saturation temperature of pure ammonia at the operating pressure of the DAR system. The highest COP is achieved at the point where the temperature at the condenser inlet (T_6) is very close to (slightly higher than) the saturation temperature of ammonia, such that the maximum flow-rate of ammonia with the minimum of water content was conveyed to the evaporator. At lower heat inputs, temperatures measured along the rectifier indicate that the condensation of ammonia occurs prior to the inlet of the condenser, thus resulting in some drain back of ammonia to the generator and a lower COP. At higher heat input rates, higher temperatures at the condenser inlet indicate that a larger fraction of water is present in the saturated vapour entering the condenser.

At the lowest heat inputs, significant subcooling is achieved at the condenser, where exit temperatures approach that of the ambient air. However, at the lowest system pressure p_{ch} = 14 bar and $\dot{Q}_{gen}$ > 250 W, Fig. 7a indicates that the fluid exiting the condenser is no longer subcooled, exiting the condenser in a two-phase state at the refrigerant saturation temperature. The uncondensed fraction of the refrigerant flow is diverted from the evaporator to the absorber via the gas bypass tube, and the result is a lower cooling output at higher values of $\dot{Q}_{gen}$ than achieved at p_{ch} = 17 bar (see Fig. 5a).

The evaporator inlet and outlet temperatures (T_9 and T_{10}, respectively) were found to vary with cooling delivery temperature more than system pressure or generator heat input. At a cooling delivery temperature of T_{cool} = 5 °C (Fig. 8a), the evaporator inlet temperature is between -22 and -25 °C across most of the heat input range, while for a cooling delivery temperature of T_{cool} = 25 °C (Fig. 8b) it is between -12 and -15 °C. In the former case, it should be noted from Fig. 8a that the evaporator outlet temperature is higher than the cooling delivery temperature due to the counterflow heat exchange with the warmer flow of hydrogen gas flowing upwards from the absorber, which enters the gas heat exchanger at the higher temperature of T_{8b}.

4.2. Experimental results – dynamic performance during system start-up

Figures 9a and 9b show generator temperature plotted against time during the start-up process, for a range of fixed heat input rates and for system charge pressures of 14 bar and 21 bar respectively. Temperature is shown to increase until the point at which the bubble pump begins to lift the solution from the generator, which is then replaced by a continuous flow of lower-temperature fluid from the reservoir. The start times and peak generator start-up temperatures for the range of test conditions are presented in Fig. 10.

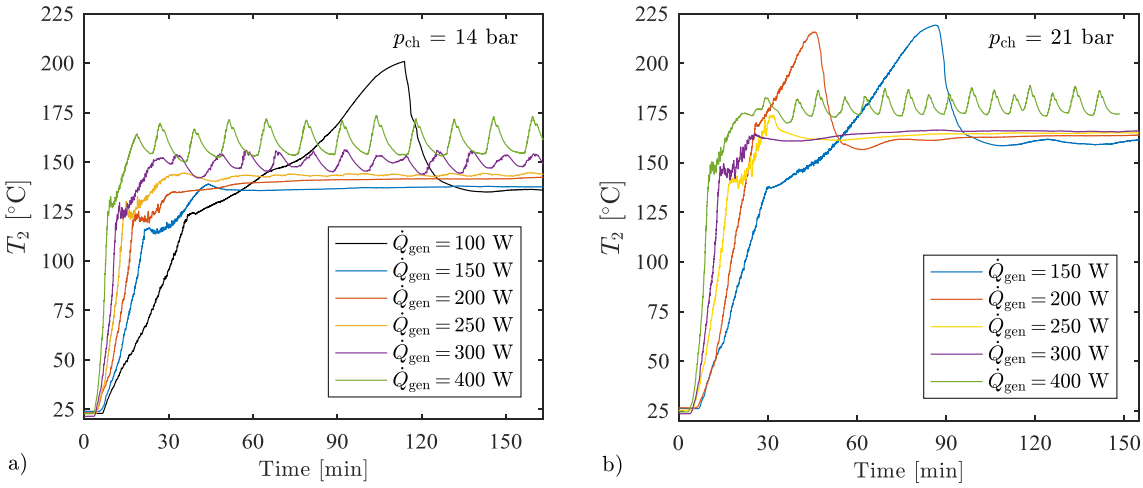

Fig. 9: Generator temperature at various steady heat input rates during start-up for: (a) 14 bar and (b) 21 bar charge pressure.

The lowest values of $\dot{Q}_{gen}$ are characterized by an "overshoot" of the generator temperature followed by a sudden drop in temperature as the system transitions to steady-state operation. Meanwhile, for the highest values of $\dot{Q}_{gen}$, an oscillating behaviour is observed for the generator temperature after the transition to steady-state. At intermediate values of $\dot{Q}_{gen}$ corresponding to peak COP, neither of these aforementioned behaviours are observed. In all cases there is a noticeable change in the rate of increase of the generator temperature during the initial heating of the solution that represents the onset of boiling, after which the temperature continues to increase at a slower rate (as is characteristic for non-isothermal phase-change processes in two-component mixtures) until the start of the bubble pump operation.

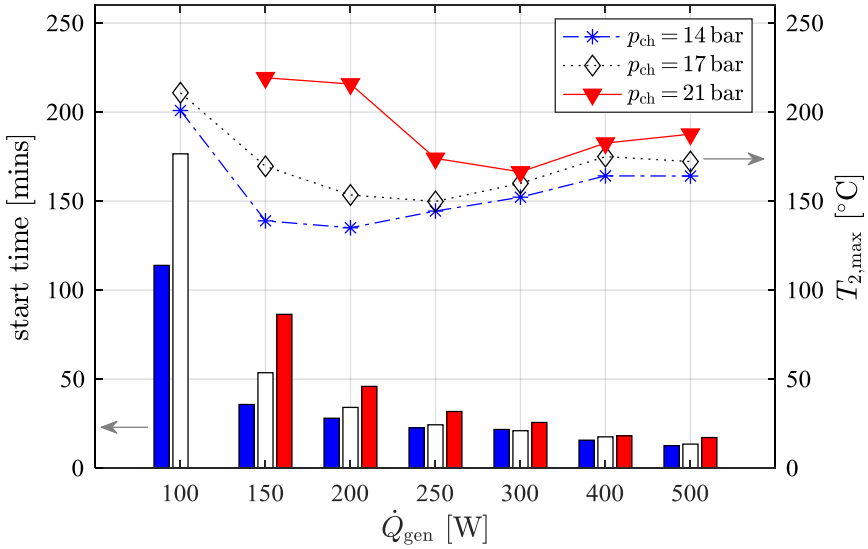

Fig. 10: Experimental results showing start-up time (bar plots) and peak generator start-up temperature (line plots) at various steady heat input rates. Shown for system charge pressures of 14 bar (blue), 17 bar (white) and 21 bar (red).

The peak in temperature observed at low values of $\dot{Q}_{gen}$ is significant. At p_{ch} = 14 bar and $\dot{Q}_{gen}$ = 100 W, the generator temperature reaches a maximum value of 201 ºC, which is 65 ºC above the temperature observed during steady-state operation. A likely reason for this is that slow nucleate boiling of stagnant fluid in the generator under low heat-flux conditions leads to a depletion of ammonia from the solution. This gradually raises the temperature at which the coalescence of bubbles is sufficient to lift liquid solution upwards in the bubble pump, before cooler solution can flow from the reservoir. At higher values of $\dot{Q}_{gen}$, there is a faster transition from nucleate boiling to flow boiling before significant depletion of the ammonia-rich solution occurs, with the result that no observable overshoot of the generator temperature occurs.

4.3. Model calibration

The results of the steady-state experiments were used to calibrate the system model. Table 1 contains a list of relations that were used to determine the state of the system according to certain environmental parameters or operational settings. The DAR system pressure p at each time instant in the model is determined as a function of the initial charge pressure p_{ch} and the generator temperature T_2. An additional equation is also included to describe the relationship between $\dot{Q}_{\mathrm{gen}}$, T_2 and p based on the experimental data. The conductance value $(UA)_{\mathrm{sc-gen}}$ describing the heat transfer between the solar heat pipe collectors and the generator was estimated from observations of the temperature difference between the cartridge heaters and generator during the tests. The parameters C and $(UA)_{\mathrm{gen-amb}}$ were estimated from the time constant of the temperature response of the generator during start-up and after shut-down. The conductance value $(UA)_{\mathrm{cond}}$ was estimated using temperature profiles measured along the two-phase (condensation) and single-phase (subcooling) zones of the condenser.

Figure 11 shows that the calibrated model gives a reasonably good prediction of cooling output, particularly at the lower end of the range of $\dot{Q}_{\mathrm{gen}}$ values, and correctly captures the trend of the COP curve. However, at higher values of $\dot{Q}_{\mathrm{gen}}$ (beyond those corresponding to the peak COP) the model is shown to over-predict $\dot{Q}_{\mathrm{evap}}$ by ~10% at $p_{\mathrm{ch}} = 14$ bar, and under-predict $\dot{Q}_{\mathrm{evap}}$ by ~15% at $p_{\mathrm{ch}} = 21$ bar.

Tab. 1: Supplementary equations and input parameters used in the solar-DAR system model.

Parameter	Value / Equation
p	$p = p_{\mathrm{ch}} + 0.123 \times 10^{-3} \cdot (T_2 - 25)^2$
$\dot{Q}_{\mathrm{gen}}$	$\dot{Q}_{\mathrm{gen}} = 14.2\,T_2 + 34.8\,p - 1293$
$\varepsilon_{\mathrm{rect}}$	$\varepsilon_{\mathrm{rect}} = 0.85$
$(UA)_{\mathrm{cond}}$	$(UA)_{\mathrm{cond}} = 5.5$
$(UA)_{\mathrm{sc-gen}}$	$(UA)_{\mathrm{sc-gen}} = 5$
$(UA)_{\mathrm{gen-amb}}$	$(UA)_{\mathrm{gen-amb}} = 0.3$
T_9	$T_9 = T_{\mathrm{cool}} - 28$
T_{10}	$T_{10} = T_9 + 37$
T_{11}	$T_{11} = T_{\mathrm{amb}} + \left(2.406 + 36.7\dot{Q}_{\mathrm{gen}}/1000\right)$
T_{8b}	$T_{8b} = T_{11} - 0.5(T_{11} - T_{\mathrm{a}})$
$\dot{Q}_{\mathrm{bp,loss}}$	$\dot{Q}_{\mathrm{bp,loss}} = \dot{Q}_{\mathrm{gen}}\left(0.65 + 0.025p - 0.0039\dot{Q}_{\mathrm{gen}}\right)$
$T_{\mathrm{gen,min}}$	$T_{\mathrm{gen,min}} = 85 + 3.6p_{ch}$
$T_{\mathrm{gen,start}}$	$T_{\mathrm{gen,start}} = 90 + 10.3p_{\mathrm{ch}} - 0.536\dot{Q}_{\mathrm{gen}}$

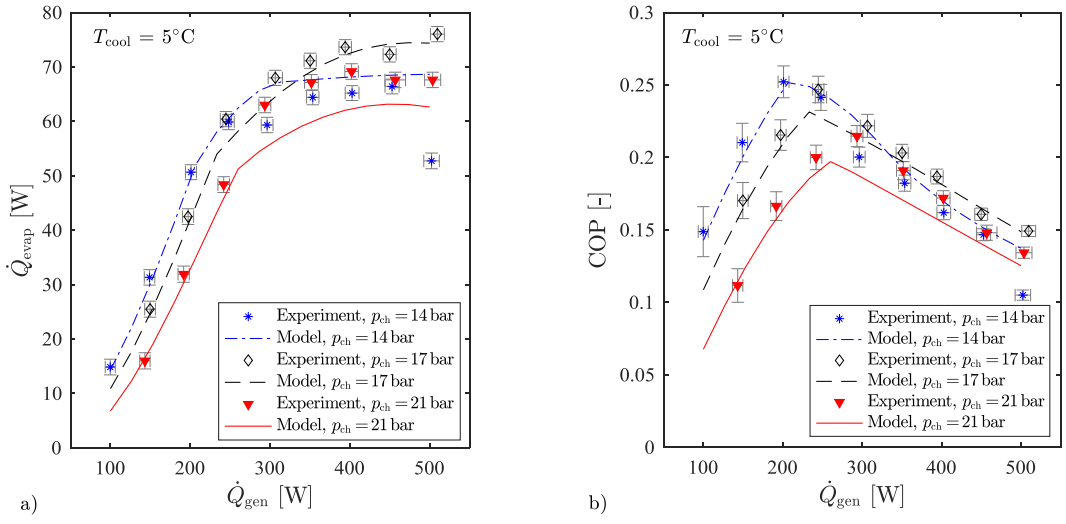

Fig. 11: Line plots showing predictions of (a) cooling power output and (b) COP from the calibrated DAR system model, overlaid with experimental data points for the corresponding charge pressures and heat input rates.

4.4. Solar-DAR system performance simulation

The solar-DAR system model, with the calibration parameters listed in Table 1 as inputs, was used to simulate the performance of the solar-DAR system on a "peak solar" day in Chennai, India. From the climate dataset, the maximum solar irradiation was found to occur on 3rd May. The peak ambient air temperature on this day is 39 ºC. Diurnal simulations were performed at system charge pressures between 12-21 bar and a delivered cooling temperature of 5 ºC. The solar collector array area was varied between 0.5-5 m^2, using Collector Types 1 and 2 presented in Section 3.2.

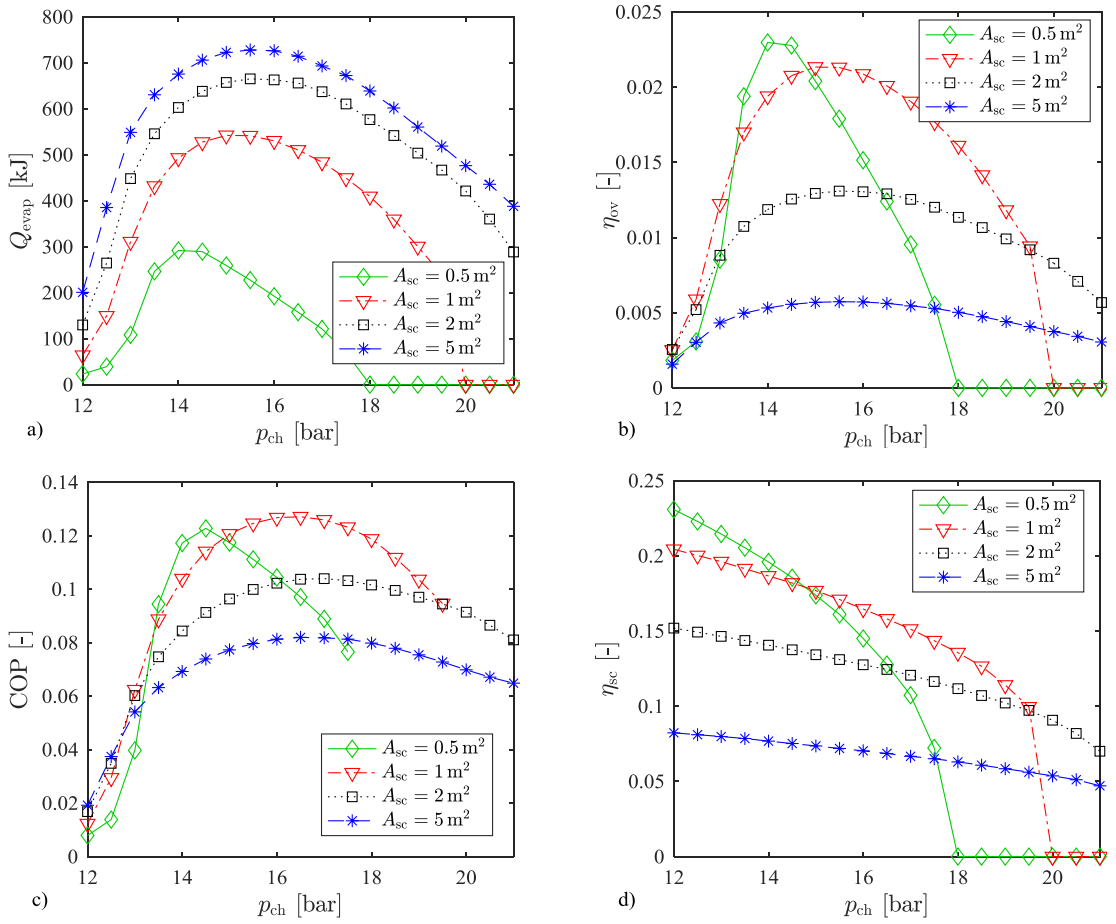

Fig. 12: Diurnal simulation results for the solar-DAR system with Collector Type 2, showing (a) total cooling output, (b) overall (solar to cooling) efficiency, (c) refrigeration cycle COP and (d) solar collector efficiency, plotted against DAR system charge pressure. Simulations are performed with various collector array areas, and a cooling delivery temperature of 5 °C.

The plots in Fig. 12a show the total daily cooling energy delivered with Collector 2 over the range of operating pressures and collector areas. As expected, cooling output increases with solar collector area, however for each doubling of the array size beyond 1 m^2, the improvement in maximum cooling output becomes smaller, indicating a higher cost per unit of cooling energy delivered; while maximum cooling output occurs at progressively higher system pressures as the array size is increased. Figure 12b shows that a maximum overall (solar to cooling) efficiency of 2.3% is achieved with 0.5 m^2 of collector array and a system pressure of 14 bar. For 1 m^2 of collector array area, a slightly lower maximum overall efficiency is achieved, however the system is able to operate over a wider range of system pressures and the DAR operates with a slightly higher COP, delivering an average power of 26 W over a 5.8 hour operating period. Figure 12c shows that with 1 m^2 of collector a DAR daily COP of up to 12.7% is achieved for a system pressure 16.5 bar. It can be seen in Fig. 12d that as system pressure is increased, the solar collector efficiency decreases due to higher collector temperatures and shorter operating periods of the DAR system; while larger collector array areas are needed to provide sufficient heat to the generator. Thus, from these results it can be predicted that an "optimal" summer-day configuration for the DAR system in Chennai is between 14-16.5 bar, with a collector array area of 0.5-1 m^2.

The simulated performance of the solar-DAR system was considerably poorer with Collector 1, delivering less than 25% of the daily cooling energy predicted with Collector 2 for an equivalent collector array area. Furthermore with Collector 1, a minimum array area of 2 m^2 was required in order to deliver sufficient thermal energy to start the system; while with an array area up to 10 m^2 the system could only operate at pressures < 14 bar.

Figures 13a and 13b show profiles of the system temperatures and energy flows over the diurnal operating period for the solar-DAR system charge pressure of 14 bar and 19 bar respectively, and with a 1 m^2 array area of the higher efficiency solar collectors (Collector Type 2) as the heat source. The figures illustrate the trade-off between the lower operating temperatures, higher collector efficiency, and longer operational period achieved at the lower system pressure; compared to the higher cooling power output during the middle of the day achieved at the higher system pressure. It can also be observed in Fig. 13a that at 14 bar the lower saturated liquid temperature of the working fluid in the condenser (shown by the green line) results in only partial condensation of the working fluid under the warm ambient conditions. As a result, 40% of the mass-flow of refrigerant bypasses the evaporator, resulting in a significant loss of cooling potential illustrated by the energy flow $\dot{Q}_{gb} = X_7 \dot{m}_r \Delta h_{fg}$. At the higher system pressure of 19 bar in Fig. 13b, the difference between the saturated liquid temperature of the working fluid in the condenser and the temperature of the ambient air is larger and therefore for most of the operating period, full condensation is achieved.

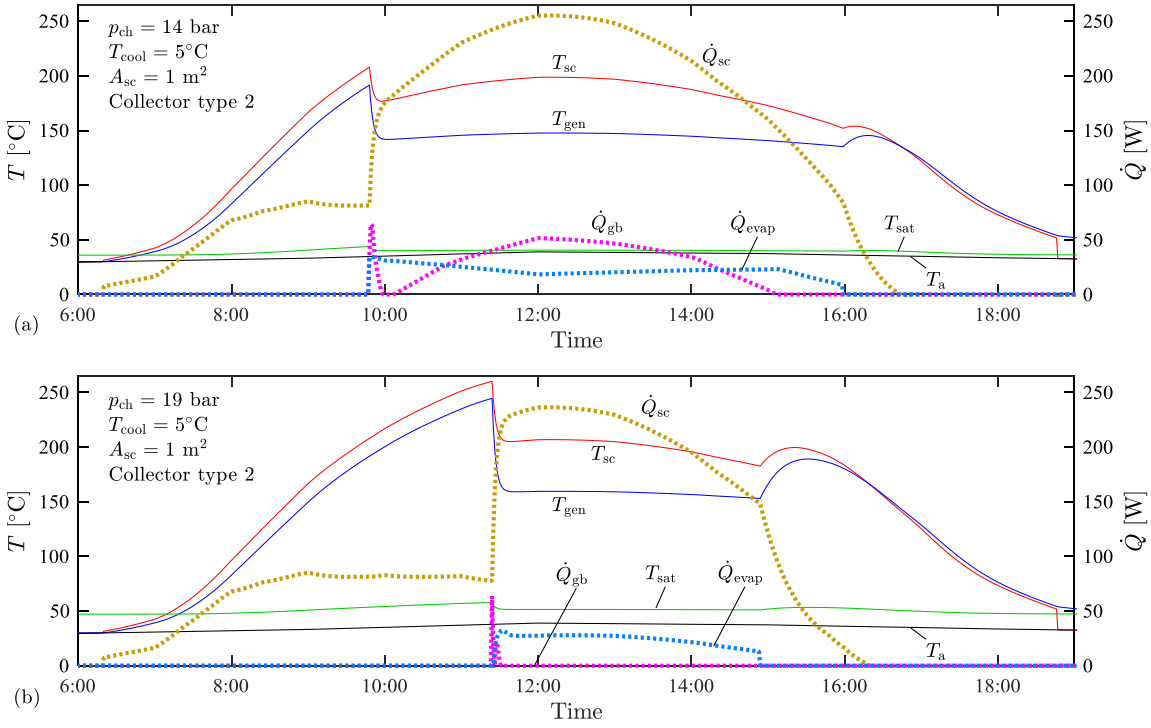

Fig. 13: Diurnal simulation profiles showing system temperatures and energy flow rates for two configuration cases.

5. Conclusions

A solar-cooling system based on a diffusion absorption refrigeration (DAR) cycle was presented, using heat-pipe solar collectors as the heat source. Based on experimental results from a DAR system operating over a range of charge pressures and heat input rates, a thermodynamic model was calibrated and used to simulate the system's performance in the climate of Chennai, India. The experimental analysis has shown that the DAR system can operate over a wide range of heat input rates, but that the maximum COP achieved is highly dependent on the system pressure. As the system pressure was lowered, a higher maximum COP was obtained for a lower corresponding generator heat input rate. For a cooling delivery temperature of 5 ºC and a charge pressure of 14 bar, a maximum COP of 0.25 was obtained with a heat input of 200 W. The observations relating to the condenser have shown that there is a limit to how far the lowering of the system pressure results in an increase in the COP of the system. This has further implications for the application of the system in the high-

ambient temperature environment of Chennai; the diurnal simulation of the solar-DAR system demonstrated that the optimal setting for the system pressure is a trade-off between reducing the generator temperature required to start the system and maximising the ability to reject heat in the condenser. Future work should investigate the effect of changing the ammonia-water solution concentration, while the diurnal simulation of the solar-DAR system should be extended to an annual analysis. The performance of this system in other geographical locations of interest with lower ambient temperatures should also be investigated.

6. Acknowledgement

This work was supported by Innovate UK and the UK Engineering and Physical Sciences Research Council (EPSRC) [grant number EP/P030920/1]. The authors would also like to thank Prof. R. Saravanan and S. Venkatakrishnan at Anna University, Chennai. Data supporting this publication can be obtained on request from cep-lab@imperial.ac.uk.

7. References

Acuña, A., Velázquez, N., Cerezo, J., 2013. Energy analysis of a diffusion absorption cooling system using lithium nitrate, sodium thiocyanate and water as absorbent substances and ammonia as the refrigerant. Appl. Therm. Eng. 51(1), 1273-1281.

ASHRAE, 2001. International Weather for Energy Calculations (IWEC) Weather Files. Available: https://energyplus.net/weather [Accessed 6 October 2017].

Ben Ezzine, N., Garma, R., Bellagi, A., 2010. A numerical investigation of a diffusion-absorption refrigeration cycle based on R124-DMAC mixture for solar cooling. Energy. 35(5), 1874-1883.

Ben Jemaa, R., Mansouri, R., Bellagi, A., 2016. Dynamic testing and modeling of a diffusion absorption refrigeration system. Int. J. Refrig. 67, 249-258.

Chen, J., Kim, K.J., Herold, K.E., 1996. Performance enhancement of a diffusion-absorption refrigerator. Int. J. Refrig. 19(3), 208-218.

Freeman, J., Ramos, A., MacDowell, N., Markides. An experimentally validated model of a solar-cooling system based on an ammonia-water diffusion-absorption cycle. The 8th International Conference on Applied Energy – ICAE2016, October 8-11, 2016, Beijing, China.

Mazouz, S., Mansouri, R., Bellagi, A., 2014. Experimental and thermodynamic investigation of an ammonia/water diffusion absorption machine. Int. J. Refrig. 45, 83-91.

Patek, J., Klomfar, J., 1995. Simple functions for fast calculations of selected thermodynamic properties of the ammonia-water system. Int. J. Refrig. 18(4), 228-234.

Shelton, S.V., White, S., 2002. Bubble pump design for single pressure absorption refrigeration cycles. ASHRAE Trans. 108, 1-10.

SPF Institute for Solar Energy, 2009. Thermostrom Strebel AS 100 HP16. Solar collector factsheet C1112. Available: www.solarenergy.ch [Accessed 6 October 2017].

Starace, G., De Pascalis, L., 2012. An advanced analytical model of the Diffusion Absorption Refrigerator cycle. Int. J. Refrig. 35(3), 605-612.

Taieb, A., Mejbri, K., Bellagi, A., 2016. Detailed thermodynamic analysis of a diffusion-absorption refrigeration cycle. Energy, 115, pp.418-434.

Von Platen, B.C., Munters, C.G., 1928. US Patent. US 1685764 A.

Zohar, A., Jelinek, M., Levy, A., Borde, I., 2005. Numerical investigation of a diffusion absorption refrigeration cycle. Int. J. Refrig. 28(4), 515-525.

Zohar, A., Jelinek, M., Levy, A., Borde, I., 2009. Performance of diffusion absorption refrigeration cycle with organic working fluids. Int. J. Refrig. 32(6), 1241-1246.